Article

Journal of
Nanoscience and Nanotechnology
Vol. 15, 8571–8576, 2015
www.aspbs.com/jnn

Copyright © 2015 American Scientific Publishers
All rights reserved
Printed in the United States of America

Improvement of Gas Sensing Characteristics by Adding Pt Nanoparticles on ZnO-Branched SnO_2 Nanowires

Han Gil Na, Yong Jung Kwon, Hong Yeon Cho, Sung Yong Kang, and Hyoun Woo Kim*

Division of Materials Science and Engineering, Hanyang University, Seoul 133-791, Republic of Korea

We coated zinc-oxide (ZnO)-branched tin oxide (SnO_2) nanowires with a Pt shell layer via a sputtering method and subsequently annealed the composite to generate Pt nanoparticles. The spillover effect of Pt nanoparticles was expected to play a significant role in enhancing the response. X-ray diffraction, scanning electron microscopy, and transmission electron microscopy revealed that the nanoparticles were comprised of a cubic Pt phase. A sensing test with NO_2 gas revealed that the sensor response to NO_2 gas was significantly increased, being related to the spillover effect of the Pt nanoparticles. As a result of the Pt-functionalization, the sensor response time and recovery time were decreased and increased, respectively. The high sensor response and fast response time make Pt-functionalized ZnO branched nanowires a promising candidate for gas sensors. The present work will be useful in exploring new areas of multiple-component nanosystems.

Keywords: Branched Nanowires, ZnO, Pt Nanoparticles, Chemical Sensors.

Delivered by Publishing Technology to: Hanyang University Library
IP: 166.104.133.64 On: Tue, 22 Sep 2015 01:33:59
Copyright: American Scientific Publishers

1. INTRODUCTION

With nanostructures attracting enormous attention because of their fascinating properties,[1–16] one-dimensional (1D) nanostructures including nanowires have been intensively studied as attractive candidates for gas sensors.[17–23] In particular, the branched nanowires have drawn great interest, for several reasons.[24] First, they have the advantages of 1D nanowires. For example, they have a directional path of charge transportation, which reduces carrier diffusion lengths and enhances electrical transport.[25, 26]

Second, three-dimensional (3D) branched nanowires exhibit the largest surface area, which maximizes the amount of reactants involved in surface reactions, which can be expected to amplify a sensing signal and to enhance sensing performance. Third, the branched nanowires have homojunctions or heterojunctions between the stem nanowires and the branches. Accordingly, the junctions add depletion regions which, further increase the changes in resistance and thus enhance the sensing behavior. Fourth, the 3D branched structures have a lot of networked ZnO homojunctions, because numerous branches have a high probability of touching each other. Accordingly, these homojunctions will provide additional sites of resistance changes, and their sensing capabilities will be greatly improved.

Up to the present, branched nanowires have been scrutinized for a variety of applications including photochemical hydrogen generation,[27] cathodoluminescence,[28] photodetection,[29] lithium-ion battery anodes,[30] gas-phase route for dye-sensitized solar cells,[31] plasmon routers,[32] and gas sensors.[24]

In the present work, we have prepared heterogeneous branched nanowires, in which ZnO branches were grown on SnO_2 nanowires. In this case, since the fabrication of SnO_2 nanowires is a well-established process, the stem preparation can be simple and easy. Furthermore, SnO_2 nanowires can be produced on a large scale at a relatively low cost. Since the surface of the ZnO is mostly covered with branches, the sensing capabilities of the present scheme will mostly depend on the ZnO branches, rather than the stems.

Up to the present, ZnO has been implemented with metal catalysts to enhance its the gas sensing capabilities.[33–36] In this respect, transition-metal nanoparticles have attracted a great deal of attention as possible additives to the sensor.[33] First, they can increase the surface area for gas interactions. Second, they can create a metal-semiconductor interface or change the energy-band structure, contributing to the change of resistance. Third, they activate the adsorption of sensing gas and concentrate the sensing gas on the sensing materials.

*Author to whom correspondence should be addressed.

Among metal catalysts, platinum (Pt) is an especially important and active transition metal. Accordingly, a variety of techniques have been implemented to enhance the sensor behavior by using the Pt catalysts. The Pt catalysts have been added not only during the preparation process but also to the as-prepared sensor materials. For example, Pt nanoparticles were directly decorated on the surface of sensor materials.[37–39] Doping with Pt was conducted by immersing the sensor materials in a Pt-containing solution.[40] Also, a Pt-containing precursor was added to the sensor material-containing precursor during fabrication, resulting in the loading of Pt.[41]

We have investigated the structure, morphology, and sensing properties of Pt-functionalized branched nanowires, in comparison to those of unfunctionalized branched nanowires, using NO_2 as a sensing gas. Pt-functionalization of the branched structures can enhance the capability of the sensors.

2. EXPERIMENTAL DETAILS

The fabrication of ZnO-branched SnO_2 nanowires is identical to the previous work.[42] Sn powder (purity: 99.9%), which was located in a ceramic boat, was used to prepared SnO_2 nanowires.[43] Subsequently, in order to attach ZnO branches, we have coated Au layer on the SnO_2 nanowires. A turbo sputter coater with a Au target (Emitech K575X, Emitech Ltd., Ashford, Kent, UK) was utilized.[44] In terms of the Ar plasma sputtering process, the temperature, deposition time, and DC sputter current were kept to 15 s, 25 °C, and 65 mA, respectively. We generated ZnO branches on core SnO_2 nanowires, in a vertical furnace.[45] By heating the Zn powders at 500 °C, at the N_2 gas flow rate of 2 standard liters per min (slm), Zn-related vapors were evaporated to react with O_2 in ambient air.[42] At the same time, the Au layer will start to agglomerated, forming Au nanoparticles. As a result, ZnO branches started to grow on the core nanowires, in terms of the Au nanoparticles.[42]

Delivered by Publishing Technology to: Hanyang University Library
IP: 166.104.133.64 On: Tue, 22 Sep 2015 01:33:59
Copyright: American Scientific Publishers

In order to coat Pt layers, a turbo sputter coater with a Pt target (Emitech K575X, Emitech Ltd., Ashford, Kent, UK) was used.[44] In the Ar plasma sputtering process, the temperature, deposition time, and DC sputter current were kept to 15 s, 25 °C, and 65 mA, respectively, in the course of coating the as-prepared SnO_2 nanowires. Following this, the samples were annealed for 30 min at 700 °C. The flow rate of Ar was set to 2000 sccm without other gas.

Scanning electron micrograph (SEMs) images were acquired by using a Hitachi S-4200 scanning electron microscope. The phase, crystallinity, and chemical composition of the products were ascertained by X-ray diffraction (XRD; Philips X'pert MRD X-ray diffractometer) at the Korean Basic Science Institute (KBSI), transmission electron microscopy (TEM; Philips CM-200 (200 kV)), and energy-dispersive X-ray spectroscope (EDX).

The sensing experiments are analogous to those previously conducted.[46–50] In order to prepare double-layer electrodes, Ti (~200 nm) and Au (~100 nm) were sequentially sputter-deposited on the specimens using an interdigital electrode mask. The sensor response was calculated to be $R = R_g/R_a$, where R_g and R_a are the resistances measured with and without NO_2 gas, respectively.

3. RESULTS AND DISCUSSION

Figures 1(a) and (c) show SEM images of ZnO-branched SnO_2 nanowires, without and with Pt nanoparticles, respectively. They clearly exhibit the one-dimensional (1D) morphology. The images clearly show the branches with a very high density, without exposing the surface of the stem nanowires. The enlarged SEM images (Figs. 1(b) and (d)) indicate that the branches also have an 1D morphology.

Figure 2(a) shows the XRD pattern of ZnO-branched SnO_2 nanowires, without Pt nanoparticles. Nearly all diffraction peaks can be indexed to the tetragonal rutile SnO_2 phase (JCPDS card: No. 41-1445) or hexagonal ZnO phase (JCPDS card: No. 36-1451). On the other hand, Figure 2(b) shows the XRD pattern of ZnO-branched SnO_2 nanowires, with Pt nanoparticles. In addition to the diffraction peaks with respect to the hexagonal ZnO and tetragonal SnO_2 phases, there exists a peak coinciding with the (111) peak of the cubic Pt with the lattice constant of $a = 0.3923$ nm (JCPDS card: No. 04-0802). By comparing Figures 2(b) with Figure 2(a), we reveal that the cubic Pt phase has been successfully added by the sputtering process.

Figure 3(a) shows the low-magnification TEM image of the branched structures annealed at 600 °C. It is clear that the branches have been attached to the stem nanowires. Figure 3(b) shows a TEM image of a typical branch, in

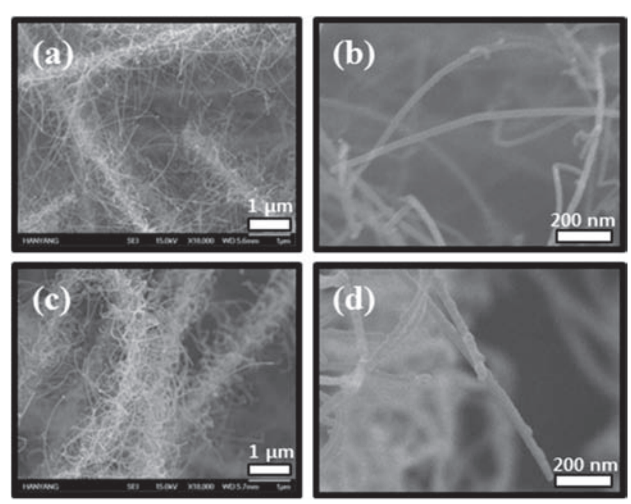

Figure 1. SEM images of ZnO-branched SnO_2 nanowires, (a), (b) without and (c), (d) with Pt nanoparticles. (b) and (d) correspond to the enlarged images of (a) and (c), respectively.

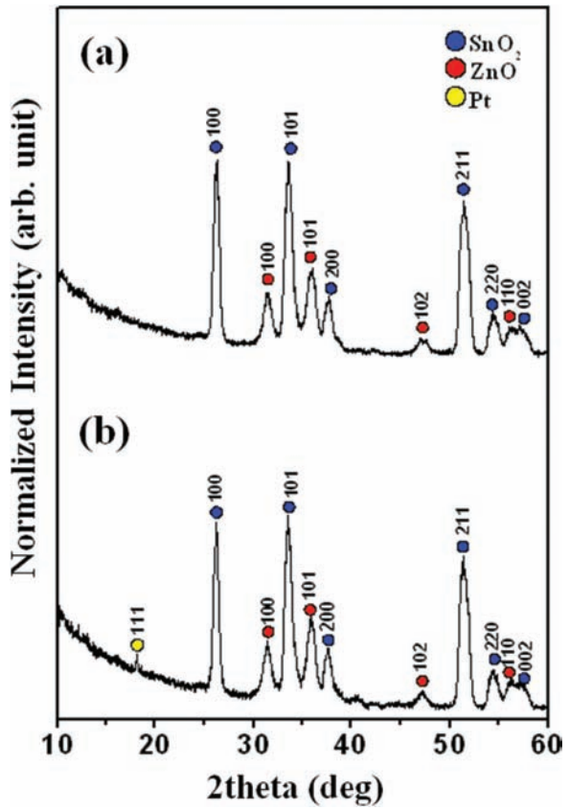

Figure 2. XRD patterns of ZnO-branched SnO_2 nanowires, (a) without and (b) with Pt nanoparticles.

Delivered by Publishing Technology to: Hanyang University Library
IP: 203.104.138.64 On: Tue, 22 Sep 2015
Copyright: American Scientific Publishers

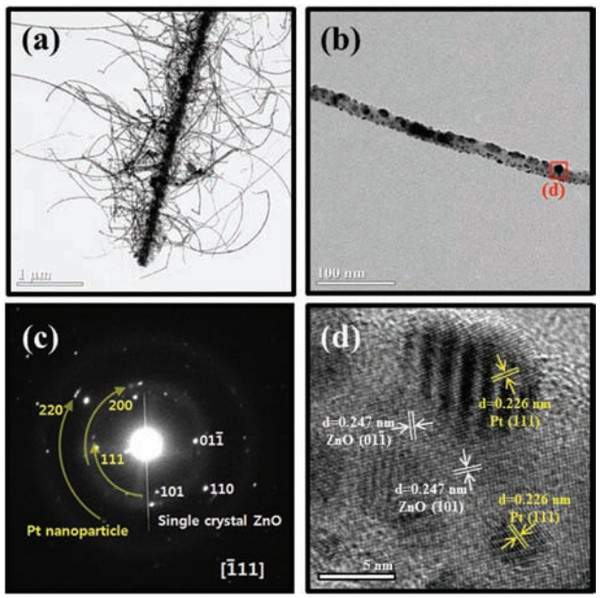

Figure 3. (a) Low-magnification TEM image of Pt-coated branched nanowires. (b) TEM image of a branch exhibiting Pt-related nanoparticles. (c) Associated SEAD pattern. (d) Lattice-resolved TEM images of the branch region.

which a lot of dark nanoparticles are decorated on the surface of the bright branch. Figure 3(c) shows an associated SAED pattern, which was observed along the [1$\bar{1}$1] axis of hexagonal ZnO. There exists a set of single-crystal electron diffraction spots of the hexagonal ZnO branches, corresponding to {01$\bar{1}$}, {101}, and {110} lattice planes of ZnO. In addition, there exists diffraction rings corresponding to the {200}, {200}, and {111} lattice plane of cubic Pt. Figure 3(d) shows a lattice-resolved TEM image of the branch region. In the branch region without nanoparticles, the spacing between the lattice planes is nearly 0.247 nm, coinciding with the d_{011} and d_{101} spacings of hexagonal ZnO. In the nanoparticle region, the interplanar spacing is approximately 0.226 nm, being associated with the (111) plane of cubic Pt.

Figure 4 shows the size distribution if Pt nanoparticles, obtained from numerous TEM images. The diameter ranged from 2–16 nm, with average diameter being estimated to be ~5.2 nm. Figure 5(a) shows a typical TEM image of branch. Figures 5(b)–(d) correspond to the elemental maps of Pt, Zn, and O elements, respectively. Elemental maps reveal that the Pt nanoparticles are present on the ZnO branches.

Figures 6(a) and (b) show the dynamic response curves of the sensors fabricated from ZnO-branched SnO_2 nanowires, without and with Pt nanoparticles, respectively. The NO_2 gas with a concentration of 2 ppm was introduced. During the sensing test, resistance increases and decreases, respectively, upon exposure to and upon removal of NO_2. It is noteworthy that the sensing response curves exhibit the saturation or the plateau probably due to the sufficiency of the sensing measurement time. Figure 6(c) compares the sensor responses of two samples, revealing that the sensor responses of ZnO-branched SnO_2 nanowires, without and with Pt nanoparticles, respectively, are 1.52 and 1.93. Accordingly, the sensor response was significantly enhanced by the Pt functionalization. Figure 6(d) shows that the response and recovery times of unfunctionalized sample are 303 and 473 s, respectively.

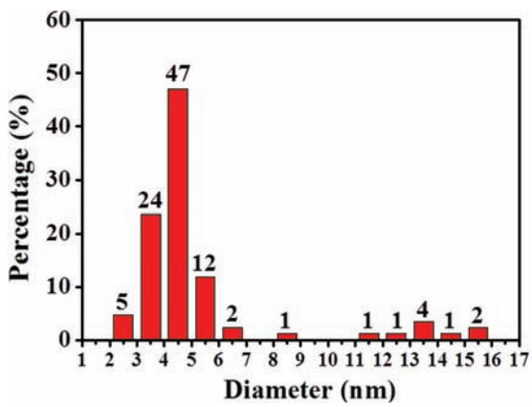

Figure 4. Distribution of Pt nanoparticles.

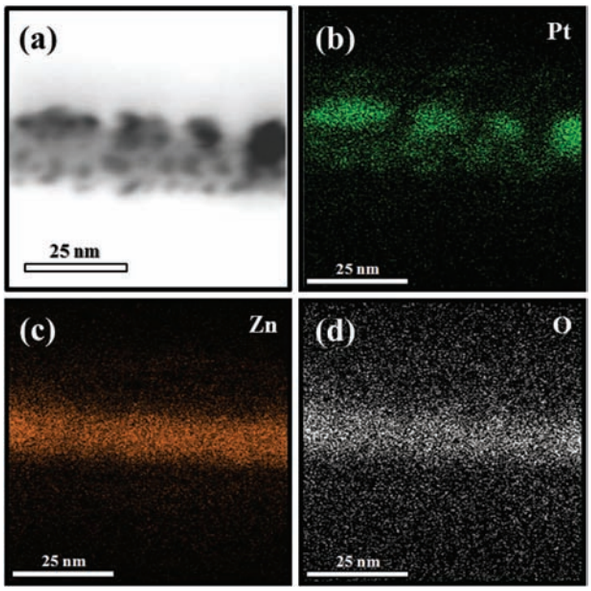

Figure 5. (a) Typical TEM image of a branch and corresponding elemental maps of (b) Pt, (c) Zn, and (d) O elements.

On the other hand, the response and recovery times of functionalized sample are 226 and 727 s, respectively.

Figure 7 shows schematic outlines of the gas sensors with the branched nanowires, with and without the Pt-functionalization. Close examination of SEM and TEM images reveal that the ZnO branches are densely formed on the SnO_2 stem nanowires. Accordingly, the SnO_2 surfaces are seldom exposed to air ambient, ZnO surface will be a main sensing material in the present work. The NO_2 sensing mechanism of the metal oxide semiconductors including ZnO has been intensively studied. NO_2

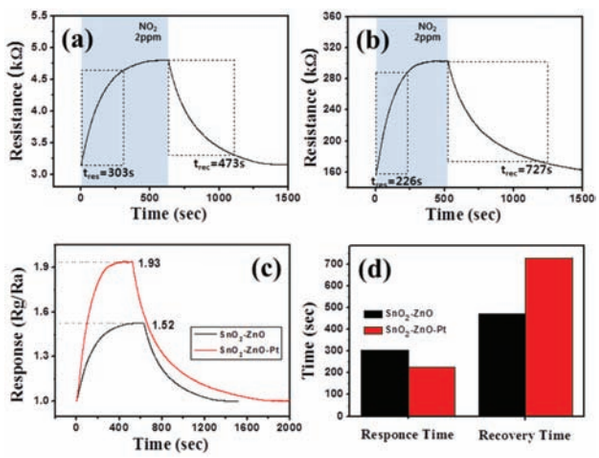

Figure 6. Response curves to NO_2 gas with a concentration of 2 ppm at 250 °C for the sensors fabricated from ZnO-branched SnO_2 nanowires, (a) without and (b) with Pt nanoparticles. (c) Response and recovery times of ZnO-branched SnO_2 nanowires, without and with Pt nanoparticles. (d) Sensor responses of ZnO-branched SnO_2 nanowires, without and with Pt nanoparticles.

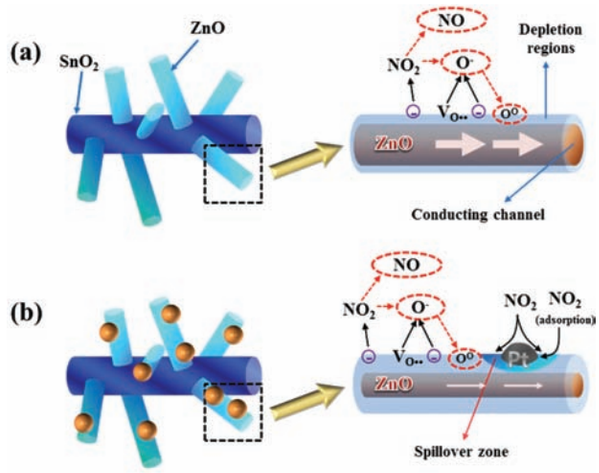

Figure 7. Schematic outlines of the sensing mechanisms with respect to branched nanowires (a) without and (b) with the Pt-functionalization.

molecules adsorbed on the ZnO surface will take electrons, resulting in the surface depletion and thus the increase of resistance (Fig. 7(a)). For example, the electrons are extracted from the conduction band of ZnO by the reaction of $NO_2 + e^- \rightarrow NO + O^-_{abs}$. It raises the resistivity of the ZnO branches.[51] On the other hand, the desorption of NO_2 molecules will cause the decrease of the sensor resistance.

We speculate the possible mechanism, by which the Pt-functionalization enhances the sensing behavior. Since the thermal annealing is included in the Pt-functionalization step, it is possible that structural defects, including oxygen vacancies, are generated. However, these defects will not contribute significantly to the change of the increase of the sensor resistance, because the surface area of ZnO, which is exposed to air ambient, will be very small, being compared to that of the unfunctionalized sample. It is noteworthy that the sensor volume near the surface only is closely related to the change of sensing performance.

Accordingly, we realize that the enhancement of sensing behavior by the functionalization will be originated from the addition of nanoparticles with a pure cubic Pt phase. In terms of a chemical sensitization, Pt promotes the dissociation of NO_2 into ionized and/or non-ionized species. By the spillover effect, the dissociated species will move to ZnO surfaces, contributing to the increase of the resistivity (Fig. 7(b)). As for an electronic sensitization, there happens to be an electron transfer between Pt and ZnO, generating the depletion region in the ZnO side beneath the Pt nanopartilces and thus increasing the change of resistance (Fig. 8). In more detail, the work functions of *n*-ZnO and Pt are 5.2 and 6.1 eV, respectively.[52, 53] Accordingly, to align the Fermi level, electrons will flow from *n*-ZnO to Pt, with the electrostatic potential of the semiconductor being raised. The Schottky barrier or interface voltage will appear at the Pt/ZnO junctions.[54, 55] Similarly, the concept of metal/ZnO Schottky barrier was introduced in the

Delivered by Publishing Technology to: [illegible]
IP: 166.104.133.64 On: Tue, 25 Aug 2015 [illegible]
Copyright: American Scientific Publishers

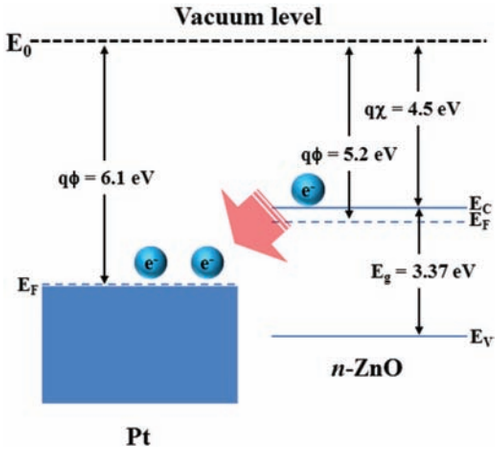

Figure 8. Energy band diagram of the Pt–ZnO system before equilibrium; bandgap energy of ZnO = 3.4 eV,[60] electron affinity of ZnO = 4.5 eV,[52] work function of ZnO = 5.2 eV,[53] and work function of Pt = 6.1 eV.[52] The energy band diagram is not drawn to scale.

previous reports.[56,57] In this case, as a result of electron flow, the depletion regions will appear on both sides of the heterojunctions. Particularly on the *n*-ZnO side, the electron depletion region will be generated. Upon the introduction of NO_2 gas, the adsorved NO_2 molecules will take out electrons from the Pt surface, ultimately resulting in the enlargement of the electron depletion region in ZnO underneath the Pt nanoparticles. The sensitivity will be enhanced, not only by the reduction of ZnO conduction volume through the generation of depletion region, but also by the resistance modulation of the heterojunctions.

Figure 6(d) indicates that the recovery time is longer than the response time, regardless of Pt-functionalization. It is generally accepted that there are high-energy and low-energy binding sites on the ZnO surfaces. Since high-energy binding sites facilitate the high adsorption but low desorption rates, we surmise that they played a role in the present case. Similarly, Yang et al. revealed that the slow desorption rate of NO_2 gas compared with the fast adsorption rate can be related to defective sites on the surface, in pristine graphene.[58,59]

The response and recovery times became shorted and longer, respectively, by the Pt-functionalization. First, it is possible that the ratio of high-energy to low-energy binding sites increases by means of the Pt-metallization. Accordingly, the NO_2 molecules will be easily adsorbed but hardly detached; the recovery and response times increases and decreases, respectively. Second, there will be a lot of high-energy binding sites on the surface of Pt nanoparticles, promoting the efficient adsorption of NO_2 species. However, these sites tend to retard the desorption of NO_2 species, being consistent with the increase of recovery time by the Pt-metallization. In addition, this phenomenon may be associated with an increase in the catalytic particle-ZnO potential barrier upon NO_2 desorption.

4. CONCLUSION

We have successfully prepared Pt-decorated ZnO-branched nanostructures, by means of growing ZnO branched nanostructures on as-synthesized SnO_2 nanowires. The Pt nanoparticles were prepared by DC sputtering and subsequent thermal annealing. XRD, SAED, and lattice-resolved TEM images coincidentally indicate that the nanoparticles are comprised of a cubic Pt phase. The sensor measurements revealed that the sensor response to NO_2 gas was increased by 27%, by the Pt-functionalization. Furthermore, the Pt-functionalization increased the response time and decreased the recovery time, respectively. The responsible mechanism is surmised to correspond to the spillover effect of Pt nanoparticles.

Acknowledgment: This research was supported by Basic Science Research Program through the National Research Foundation of Korea (NRF) funded by the Ministry of Education, Science and Technology (2011-0009946).

References and Notes

1. A. Sarkar, K. Kanakamedala, N. N. Jagadish, A. Jordan, S, Das, N. Siraj, I. M. Warner, and T. Daniels-Race, *Electron. Mater. Lett.* 10, 879 (**2014**).
2. Y. A. K. Reddy, B. Ajitha, P. S. Reddy, M. S. P. Reddy, and J.-H. Lee, *Electron. Mater. Lett.* 10, 907 (**2014**).
3. S. Kim, G. Nam, and J.-Y. Leem, *Electron. Mater. Lett.* 10, 915 (**2014**).
4. S. B. Jambure, G. S. Gund, D. P. Dubal, S. S. Shinde, and C. D. Lokhande, *Electron. Mater. Lett.* 10, 943 (**2014**).
5. H.-A. Choi, H. Jang, H. Hwang, M. Choi, D. Lim, S. E. Shim, and S.-H. Baeck, *Electron. Mater. Lett.* 10, 957 (**2014**).
6. N. K. Singh, B. Choudhuri, A. Mondal, J. C. Dhar, T. Goswami, S. Saha, and C. Ngangbam, *Electron. Mater. Lett.* 10, 975 (**2014**).
7. J. S. Maeng, D. J. Choi, K.-O. Ahn, and Y.-H. Kim, *Electron. Mater. Lett.* 10, 1019 (**2014**).
8. L. R. Shobin and S. Manivannan, *Electron. Mater. Lett.* 10, 1027 (**2014**).
9. M. Zhuang, A. Wei, J. Liu, Y. Zhao, and Z. Yan, *Electron. Mater. Lett.* 10, 1075 (**2014**).
10. S.-K. Kim, C. J. Raj, and H.-J. Kim, *Electron. Mater. Lett.* 10, 1137 (**2014**).
11. R. Yu, J.-H. Pee, H.-J. Kim, and Y. J. Kim, *Electron. Mater. Lett.* 10, 1159 (**2014**).
12. Y.-S. Cho and Y.-D. Huh, *Electron. Mater. Lett.* 10, 1185 (**2014**).
13. Y. D. Jo, S. Lee, J. Seo, S. Lee, D. Ahn, and H. Lee, *J. Nanosci. Nanotechnol.* 14, 9148 (**2014**).
14. Y. K. Kin, S. Cha, J. H. Lee, and S. H. Hong, *J. Nanosci. Nanotechnol.* 14, 9143 (**2014**).
15. K. S. Min, K. S. Kim, K. N. Kim, A. Mishra, and G. Y. Yeom, *J. Nanosci. Nanotechnol.* 14, 9108 (**2014**).
16. J. H. Son, Y. H. Song, B. J. Kim, and J.-L. Lee, *Electron. Mater. Lett.* 10, 1171 (**2014**).
17. N. S. Ramgir, Y. Yang, and M. Zacharias, *Small* 6, 1705 (**2010**).
18. Y. Hu, J. Zhou, P.-H. Yeh, Z. Li, T.-Y. Wei, and Z. L. Wang, *Adv. Mater.* 22, 3327 (**2010**).
19. M.-W. Ahn, K.-S. Park, J.-H. Heo, J.-G. Park, D.-W. Kim, K. J. Choi, J.-H. Lee, and S.-H. Hong, *Appl. Phys. Lett.* 93, 263103 (**2008**).
20. Q. Kuang, C. Lao, Z. L. Wang, Z. Xie, and L. Zheng, *J. Am. Chem. Soc.* 129, 6070 (**2007**).

Delivered by Publishing Technology to: [illegible]
IP: [illegible] Tue, 22 Sep 2015 01:33:59
Copyright: American Scientific Publishers

21. M. C. McAlpine, H. Ahmad, D. Wang, and J. R. Heath, *Nat. Mater.* 6, 379 (**2007**).
22. Q. Wan, Q. H. Li, Y. J. Chen, T. H. Wang, X. L. He, J. P. Li, and C. L. Lin, *Appl. Phys. Lett.* 84, 3654 (**2004**).
23. A. Kolmakov, Y. Zhang, G. Cheng, and M. Moskovits, *Adv. Mater.* 15, 997 (**2003**).
24. Q. Wan, J. Huang, Z. Xie, T. H. Wang, E. N. Dattoli, and W. Lu, *Appl. Phys. Lett.* 92, 102101 (**2008**).
25. C. W. Cheng, W. N. Ren, and H. F. Zhang, *Nano Energy* 5, 132 (**2014**).
26. S. W. Boettcher, J. M. Spurgeon, M. C. Putnam, E. L. Warren, D. B. Turner-Evans, M. D. Kelzenberg, J. R. Maiolo, H. A. Atwater, and N. S. Lewis, *Science* 327, 185 (**2010**).
27. A. Kargar, Y. Jing, S. J. Kim, C. T. Riley, X. Q. Pan, and D. L. Wang, *ACS Nano* 7, 11112 (**2013**).
28. C. Y. Luan, T. L. Wong, and J. A. Zapien, *J. Cryst. Growth* 374, 65 (**2013**).
29. S.-B. Wang, C.-H. Hsiao, S.-J. Chang, Z. Y. Jiao, S.-J. Young, S.-C. Hung, and B.-R. Huang, *IEEE Trans. Nanotechnol.* 12, 283 (**2013**).
30. H. Wu, M. Xu, Y. Wang, and G. Zheng, *Nano Research* 6, 167 (**2013**).
31. X. Y. Hou, Y. J. Hu, H. Jiang, J. C. Huo, Y. F. Li, and C. Z. Li, *J. Mater. Chem. A* 1, 13814 (**2013**).
32. Y. R. Fang, Z. P. Li, Y. Z. Huang, S. P. Zhang, P. Nordiander, N. J. Halas, and H. X. Xu, *Nano Lett.* 10, 1950 (**2010**).
33. M. Hjiri, L. El Mir, S. G. Leonardi, A. Pistone, L. Mavilia, and G. Neri, *Sens. Actuators B* 196, 413 (**2014**).
34. M. S. Yao, F. Ding, Y. B. Cao, P. Hu, J. M. Fan, C. Lu, F. L. Yuam, C. Y. Shi, and Y. F. Chen, *Sens. Actuators B* 201, 255 (**2014**).
35. J. Guo, J. Zhang, M. Zhu, D. X. Ju, H. Y. Xu, and B. Q. Cao, *Sens. Actuators B* 199, 339 (**2014**).
36. M. M. Xu, Q. Li, Y. Ma, and H. Q. Fan, *Sens. Actuators B* 199, 403 (**2014**).
37. J. J. Chen, J. D. Zhang, M. M. Wang, and Y. Li, *Sens. Actuators B* 201, 402 (**2014**).
38. X. Y. Li, X. H. Liu, W. W. Wang, L. Li, and X. Q. Lu, *Biosens. Bioelectron.* 59, 221 (**2014**).
39. G.-J. Sun, S.-W. Choi, S.-H. Jung, A. Katoch, and S. S. Kim, *Nanotechnology* 24, 025504 (**2013**).
40. X. Chen, D. M. Li, S. F. Liang, S. Zhan, and M. Liu, *Sens. Actuators B* 177, 364 (**2013**).
41. J. X. Dai, M. H. Yang, Z. Yang, Z. Li, Y. Wang, G. P. Wang, Y. Zhang, and Z. Zhuang, *Sens. Actuators B* 190, 657 (**2014**).
42. S. S. Kim, H. G. Na, S.-W. Choi, D. S. Kwak, and H. W. Kim, *Microelectron. Eng.* 105, 1 (**2013**).
43. H. W. Kim and S. H. Shim, *J. Korean Phys. Soc.* 47, 516 (**2005**).
44. H. W. Kim, S. H. Shim, and J. W. Lee, *Carbon* 45, 2695 (**2007**).
45. H.W. Kim and N.H. Kim,*Appl. Phys. A* 80, 537 (**2005**).
46. J. Y. Park, K. Asokan, S. W. Choi, and S. S. Kim, *Sens. Actuators B* 152, 254 (**2011**).
47. S. W. Choi, J. Y. Park, and S. S. Kim, *Nanotechnology* 20, 465603 (**2009**).
48. J. Y. Park, S. W. Choi, J. W. Lee, C. Lee, and S. S. Kim, *J. Am. Ceram. Soc.* 92, 2551 (**2009**).
49. H. W. Kim, S. H. Shim, J. W. Lee, J. Y. Park, and S. S. Kim, *Chem. Phys. Lett.* 456, 193 (**2008**).
50. J. Y. Park, S. W. Choi, and S. S. Kim, *Nanoscale Res. Lett.* 5, 353 (**2010**).
51. C. Baratto, G. Sberveglieri, A. Onischuk, B. Caruso, and S. di Stasio, *Sens. Actuators B* 100, 261 (**2004**).
52. Z. L. Wang and J. H. Song, *Science* 312, 242 (**2006**).
53. X. Bai, E. G. Wang, P. Gao, and Z. L. Wang, *Nano Lett.* 3, 1147 (**2003**).
54. W. P. Kang and C. K. Kim, *Sens. Actuators B* 22, 47 (**2003**).
55. M. E. Franke, T. J. Koplin, and U. Simon, *Small* 2, 36 (**2006**).
56. Y. Zhao, X. Lai, P. Deng, Y. Nie, Y. Zhang, L. Xing, and X. Xue, *Nanotechnology* 25, 115502 (**2014**).
57. G. Neri, A. Bonavita, G. Micali, G. Rizzo, N. Pinna, and M. Niederberger, *Sens. Actuators B* 127, 455 (**2007**).
58. I.-S. Hwang, S.-J. Kim, J.-K. Choi, J. Choi, H. Ji, G.-T. Kim, G. Cao, and J.-H. Lee, *Sens. Actuators B* 148, 595 (**2010**).
59. S.-W. Choi, J. Y. Park, and S. S. Kim, *Nanotechnology* 20, 465603 (**2009**).
60. J. G. Wu, X. J. Lou, Y. Wang, and J. Wang, *Electrochem. Sol. Stat. Lett.* 13, G9 (**2010**).

Delivered by Publishing Technology to: Hanyang University Library
IP: 166.104.133.64 On: Tue, 22 Sep 2015 01:33:59
Copyright: American Scientific Publishers

Received: 23 October 2014. Accepted: 27 January 2015.